Pergamon

Atmospheric Environment Vol. 31, No. 11, pp. 1677–1688, 1997

1352-2310/97 $17.00 + 0.00

PII: S1352-2310(96)00320-2

MEASUREMENTS OF DENSITY FLUCTUATIONS IN STEADY, BUOYANT PLUMES IN CROSSFLOW

PABLO HUQ and E. J. STEWART

College of Marine Studies and Center for Applied Coastal Research, University of Delaware, Newark, Delaware 19716, U.S.A.

(*First received* 29 *May* 1996 *and in final form* 3 *October* 1996. *Published March* 1997)

Abstract—Measurements of density fluctuations in steady, buoyant plumes in crossflow are reported. The aim of the laboratory experiments is to obtain density time series within the elevated plume at various locations downwind of the source. Rms levels of density fluctuations are approximately equal in magnitude to the value of the local mean, but time series show that peak values are an order of magnitude greater than the local mean. Crosswind distributions of skewness and kurtosis show near Gaussian values at the center of the plume but indicate skewed and peaked distributions at the plumes' edges. Analysis of the conditional signal reveals that values of the intermittency and non-dimensional burst frequency are inhomogeneous; their product, the burst persistence time, is near constant, however. Evaluation of the duration and spacing between events indicates that instantaneously large density fluctuations will persist for non-dimensional distances of at least up to $x/\ell_B \sim 1000$.

Key word index: Atmospheric dispersion, laboratory modelling, density fluctuations, plumes in crossflows, turbulence.

1. INTRODUCTION

Buoyant plumes in crossflows occur frequently and consequently have been extensively studied (see review by List (1982)). Most previous studies, however, have focused on the mean concentration (or density) field. From the viewpoint of hazard assessment of accidental or controlled releases of toxic or flammable materials to the environment, it is insufficient to know only details of mean quantities due to the extreme toxicity or flammability of materials commonly used in industrial manufacturing processes. This is because acute toxicity and flammability can be important at short exposure times even at mean concentrations as small as 1% of the maximum value at the location of the source of the release. Thus, knowledge of instantaneous peak concentrations, or more generally the fluctuating concentration (or density) field, is integral in the evaluation of the nature and extent of hazards. Nonetheless, the difficulties and expense of obtaining information on elevated plumes have inhibited the acquisition of data of the fluctuating density field. The purpose of this paper is to present data on the evolution of density fluctuations in a steady, buoyant plume in a crossflow obtained from laboratory experiments. The results of analyses of density fluctuations determined by traverses through the cross-sections of the buoyant plume are presented and discussed. Thus, we are concerned with both the spatial distribution and the temporal variability of the fluctuating density field. The results pertaining to the mean density field of the steady, buoyant plume in a crossflow were reported in a companion paper (Huq and Stewart, 1996). In this paper we review previous studies on fluctuations in Section 2 and follow this with brief details of the experimental apparatus in Section 3. Results and discussion of density fluctuations appear in Section 4; conclusions appear in Section 5.

2. PREVIOUS STUDIES

Most concentration fluctuation studies examine concentration fluctuations at the ground level. This applies to both field measurements and laboratory studies. For example, the measurements in the atmosphere by Jones (1983), Hanna (1984), Sawford *et al.* (1985), Sawford (1987), Dinar *et al.* (1988), DeVaull (1990), Mylne and Mason (1991), Mylne (1993), Yee *et al.* (1993a), Jorgensen and Mikkelsen (1993), all focus on ground-level concentrations. Likewise, the principal goal of the laboratory studies of Fackrell and Robins (1982), Deardorff and Willis (1984), Bara *et al.* (1992), Yee *et al.* (1993b) was to obtain ground-level concentrations. All these investigations of fluctuations required the use of probes with small spatial resolution and fast temporal response and they have met such criteria with varying degrees of success. Briefly, the instrumentation of field studies have limited resolution: laboratory investigations, though able to achieve

statistically stationary flows if desired, have limited scale separation between the large scale eddies of the inertial sub-range and the viscous dominated small scales. None the less, a consensus exists that the scalar signal is intermittent (in time and space), and that the magnitude of the ratio of the root-mean-square concentration fluctuation non-dimensionalized by the mean concentration $c'/\bar{c}$ is of order 1.

The present study differs from most of the above in that we examine the statistics of density fluctuations of a rising buoyant plume. It differs in that the scalar field is dynamic (i.e. density rather than concentration fluctuations). Secondly, as noted by Fackrell and Robins (1982), the nature of ground-level concentration fluctuations differs in that it is associated with severely distorted turbulence in the immediate proximity of the ground. This distortion leads to vertical variations in the concentration fluctuation statistics with distance from the ground. Such variations are evident in the results both of the laboratory experiments of Fackrell and Robins (1982) and in the field measurements of Mylne (1993). The nature of fluctuations in a rising buoyant plume is hinted by the field measurements of concentration fluctuations determined from LIDAR observations of rising atmospheric plumes of Lewellen and Sykes (1986). Despite limited spatial resolution, they found that $c'/\bar{c} = O(1)$ and that there was considerable variation in the value of $c'/\bar{c}$ between the edge and centerline of the plume.

3. EXPERIMENTAL APPARATUS

The experimental setup and apparatus used in this study are identical to those described in the companion paper by Huq and Stewart (1996) which reported results of the mean density field. Thus we give only brief details of the apparatus and instrumentation and refer the reader to the above paper for further information. The experiments are undertaken in a recirculating water tunnel 400 cm long, 40 cm deep, and 25 cm wide (see Fig. 1). The flow in the tunnel is driven by centrifugal pumps, and the value of the mean crossflow velocity $\bar{U}$ is 8.3 cm s^{-1}. Ambient turbulence in the crossflow is small ($w'/\bar{U} = 0.3\%$ where w' is the root mean square vertical velocity fluctuation) so that the crossflow can be considered laminar. The plume is produced with a saline solution pumped through a brass pipe of internal diameter $d = 0.36$ cm. Thus the Schmidt number ($= \nu/\kappa$), the ratio of momentum to scalar diffusivity, is 700. The brass pipe is mounted perpendicular to the crossflow $\bar{U}$, and flow through the brass pipe is controlled by a flow meter. Fluorescent Rhodamine dye is added to the plume reservoir for flow visualization. Density measurements are made by an aspirating conductivity probe with a spatial resolution of 0.04 cm and frequency response of 70 Hz which was determined from plunge tests through a sharp density interface. Velocity measurements are made by a hot-film anemometer (Type AN1003) using an x-film quartz-coated cylindrical probes (Type TSI 1241-20W). The Froude number $F = w_s/g'd$ varied between 8.55 and 13.36, and plume source exit Reynolds number $w_s d/\nu$ ranged in 700–1000 where w_s is the source exit velocity and ν the kinematic viscosity. Data from two runs comprise the results of this paper. For these runs the values of the buoyancy length scale ℓ_B (which is defined below) are 0.077 and 0.056 cm. The source exit velocity w_s was 30 and 20 cm s^{-1}, and non-dimensional density difference $\Delta\bar{\rho}/\bar{\rho}$ was 0.0143 and 0.0155 for $\ell_B =$ 0.077 and 0.056 cm, respectively. Further values of the experimental parameters are given in Table 1 of Huq and Stewart (1996).

Note that the present study concerns discharges into a laminar crossflow. For analysis of releases to the atmosphere, the results are thus most pertinent to plume discharges into a weakly turbulent atmosphere. Measurements of the increased mixing which arises in a turbulent crossflow are presented in Huq and Stewart (1996).

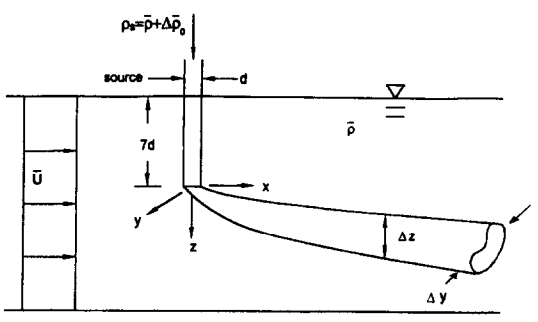

Fig. 1. Flow configuration and coordinate system.

4. RESULTS AND DISCUSSION

A length scale pertinent to the dynamics of buoyant plumes in a crossflow is ℓ_B defined as

$$\ell_b = Qg'/\bar{U}^3 \tag{1}$$

where Q is the source discharge rate, g' is the reduced gravity of the plume at the source ($g' \equiv g(\rho_s - \rho)/\rho$), and $\bar{U}$ is the mean velocity of the crossflow. The length scale ℓ_B is used to scale the results which follow. (The reader is referred to Huq and Stewart (1996) for results of the centerline trajectory of the plume, the evolution of the plume radius, mean vertical velocities and dissipation rate of plume turbulence, and mean density profiles and dilution values.)

The structure of the plume is shown in the visualization of Fig. 2. Here the plume is seen to descend as it flows from left to right. The lower boundary is more convoluted than the upper boundary, and the scale of the lower boundary convolutions grow with distance from the source due to gravitational instability. For example, at $x = 50$ cm a typical scale of convolutions is 2 cm, whereas at $x = 80$ cm the scale of the convolutions has grown to 3 cm. The structure of the plume suggests that density measurements at a point within the plume can comprise either crossflow or plume

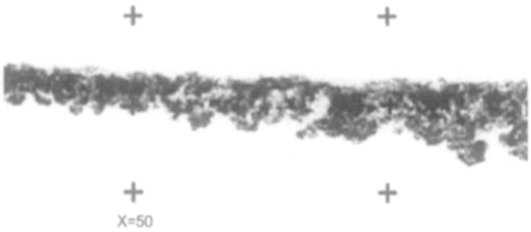

Fig. 2. Visualization of a buoyant plume in crossflow showing elevation (x–z plane) view. Flow is from left to right. Crosses mark a 30 cm grid in the x direction and 10 cm in the z direction. $\ell_B = 0.077$ cm.

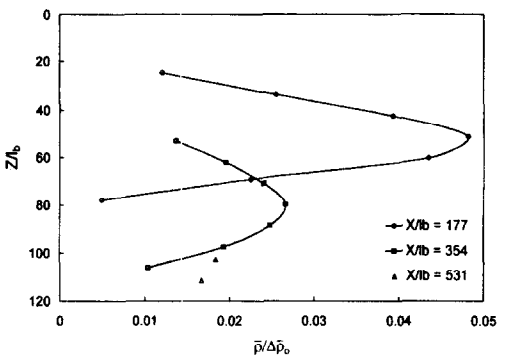

Fig. 3. Vertical profiles of mean density at plume centerline (i.e. $y = 0$) at $x/\ell_B = 177$, 354, 531. $\ell_B = 0.056$ cm.

fluid and so can be intermittent. It is likely that the degree of intermittency will increase towards the edge of the plume: this is verified below (see Figs 8, 9 and 11) by various statistical measures of the signal.

The vertical profile of the mean density through the plume is shown in Fig. 3 at three downstream locations for the case when $\ell_B = 0.056$ cm (see Table 1 of Huq and Stewart (1996) for run parameters. Note that the mean density is non-dimensionalized by the initial density difference $\Delta\bar{\rho}_0$ at the source.) The maximum density at each location occurs approximately in the middle (i.e. geometric center) of the plume. The location of the peak concentration descends with distance as expected for a descending plume (e.g. at $x/\ell_B = 177$ the peak density occurs at $z/\ell_B \sim 50$, whereas at $x/\ell_B = 354$ the peak density occurs at $z/\ell_B \sim 80$). That buoyant plumes in crossflows are strongly entraining flows is shown by the fact that values of the peak densities have decreased to 4.8 and 2.7% of $\Delta\bar{\rho}_0$ by short distances $x/\ell_B =$ 177 and 354 from the source.

The evolution of non-dimensional density fluctuations is shown in Fig. 4: here, the abscissa is the rms density fluctuation ρ' non-dimensionalized by the initial density difference $\Delta\bar{\rho}_0$ between the plume and ambient crossflow fluid at the source. The data show that peak values of density fluctuations occur near the middle of the plume. Comparison with the distribution of non-dimensional mean density $\bar{\rho}/\Delta\bar{\rho}_0$ of Fig. 3 shows, however, that the vertical distribution of the

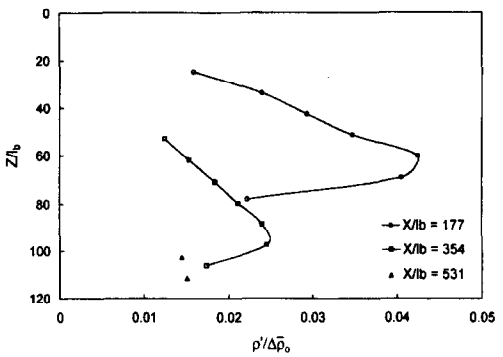

Fig. 4. Vertical profiles of rms density fluctuation at plume centerline (i.e. $y = 0$) at $x/\ell_B = 177$, 354, 531. $\ell_B = 0.056$ cm. Abscissa is non-dimensionalized by density difference at the source $\Delta\bar{\rho}_0$.

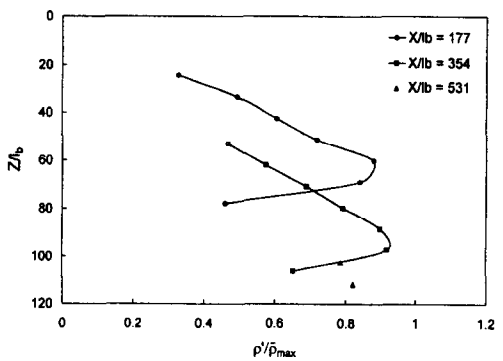

Fig. 5. Vertical profile of rms density fluctuation at plume centerline (i.e. $y = 0$) at $x/\ell_B = 177$, 354, 531. $\ell_B = 0.056$ cm. Abscissa is non-dimensionalized by maximum local mean density $\bar{\rho}_{MAX}$.

non-dimensional density fluctuation $\rho'/\Delta\bar{\rho}_0$ is not as symmetrical, and that the location of the maximum value of $\rho'/\Delta\bar{\rho}_0$ occurs closer to the lower boundary. For example, peak values of $\rho'/\Delta\bar{\rho}_0$ occur at $z/\ell_B = 60$ and 90 for the vertical sections at $x/\ell_B = 177$ and 354, respectively of Fig. 4. This gives a hint of the asymmetric mixing in the plume cross-section: later (e.g. see Fig. 9) we show indeed that statistical measures of the plume density field are not symmetrical.

Another normalization of rms density fluctuation is by the maximum value of the mean density at that longitudinal location. This is done in Fig. 5. It is evident that the vertical profiles of $\rho'/\bar{\rho}_{MAX}$ for $x/\ell_B = 177$ and 354 are similar, and that the maximum values of $\rho'/\bar{\rho}_{MAX}$ are approximately equal to 0.9. The longitudinal evolution of maximum rms density fluctuation for both normalizations is summarized in Fig. 6. Note the two ordinate scales. The ordinate on the left is $(\rho'/\Delta\bar{\rho}_0)_{MAX}$, and data are obtained from the maxima of each profile of Fig. 4: the ordinate on the right is $(\rho'/\Delta\bar{\rho}_{MAX})_{MAX}$ and data are obtained from the maxima of each profile of Fig. 5. Maximum values of rms density fluctuation as a

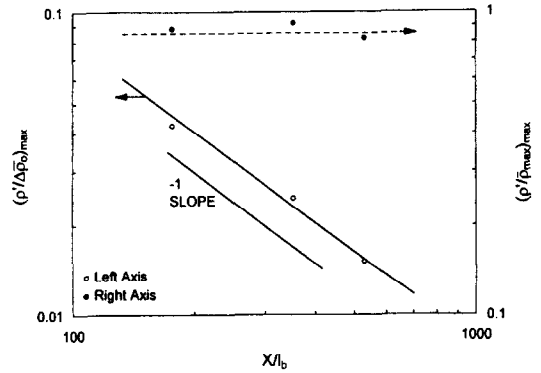

Fig. 6. Downwind evolution of rms density fluctuation at plume centerline (i.e. $y = 0$). $\ell_B = 0.056$ cm. Note the two ordinate scales. Open and closed symbols are data nondimensionalized by $\Delta\bar{\rho}_0$ and $\bar{\rho}_{MAX}$ respectively. Indicated is a -1 power law slope.

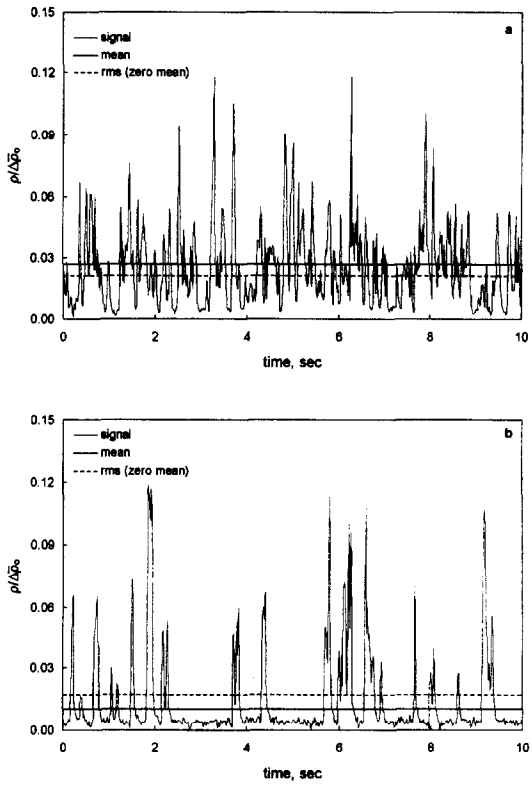

Fig. 7. Examples of time series at the plume centerline ($y = 0$) for (a) near the middle $z/\ell_B = 79$, and (b) near the edge $z/\ell_B = 106$ of a buoyant plume. Note that instantaneous peak values can be much larger than the rms or the mean. $\ell_B = 0.056$ cm. Data at $x/\ell_B = 240$.

fraction of the initial density difference decays with distance. Empirically we find

$$(\rho'/\Delta\bar{\rho}_0)_{MAX} = 8\,(x/\ell_B)^{-1} \qquad (2)$$

Equation (2) is useful in predictions e.g. a 1% intensity of rms density fluctuation is likely to occur at a distance of $x/\ell_B \sim 800$. Figure 6 also shows that the average value of the ratio $(\rho'/\bar{\rho}_{MAX})_{MAX}$ is constant and is equal to 0.85. Thus, physically, at any value of x/ℓ_B the magnitude of rms density fluctuation is similar to the magnitude of the maximum mean density at that value of x/ℓ_B.

Examination of the density time series provides further details on the nature of the density fluctuations in a buoyant plume in a crossflow. The signal is intermittent at both the middle and edge of the plume (Fig. 7a and b, respectively), and it is evident that a wide range of time scales are involved in the dynamics. (Note that the time series of which Fig. 7a and b are representative segments are 100 s long.) Also evident is that instantaneous peak values of the signals from the plume center and edge attain similar values even though the values of the mean differ. The signal in the middle of the plume contains more events, and its values for the mean and rms are 0.027 and 0.021 so that $\rho'/\Delta\bar{\rho} = 0.78$. In contrast, a significant fraction of the signal in the edge of the plume comprises very low (near zero) values occasionally interspersed with intermittent peaks, or spikes, of high density. For the signal at the edge of the plume, the relatively fewer number of events aggregate to a smaller mean, and a value of the rms fluctuation that is greater than the mean (e.g. mean = 0.010, rms = 0.018 so that $\rho'/\Delta\bar{\rho} = 1.8$). Note that at the edge the maximum values of density can reach 0.12 so that instantaneous peak values are an order of magnitude greater than the mean value.

Typical results for characterization of the intermittent signal by the third and fourth moments, skewness, and kurtosis, respectively, are presented in Fig. 8. Vertical profiles show that values of skewness and kurtosis approach near Gaussian values in the central region of the plume. Results also indicate that with distance from the center of the plume the signals rapidly become highly skewed and intermittent. For example, at the edge of the plume in the proximity of the boundary between plume and ambient crossflow fluid, values of skewness and kurtosis can be higher than 5 and 50, respectively.

The nature of the spatial distribution of the calculated statistics is more apparent in the crosswind sections (i.e. y–z plane) of Fig. 9 of the normalized (by $\Delta\bar{\rho}_0$) mean and fluctuation, skewness and kurtosis. Note that in these sections data were only collected for $y \geqslant 0$, and that there is a mirror image for negative values of y/ℓ_B (i.e. reflection about the axis $y = 0$). Both the normalized mean and fluctuation show a central region (or core) of relatively high values. Given that the maximum values of the signal are similar at the core and the edge of the plume (see Fig. 7), it is likely that the lower values of the normalized mean and fluctuation at plume's edge arise from the decreased probability of occurrence of plume fluid there. Concomitantly, higher values of skewness and kurtosis may thus be expected at the plume edge.

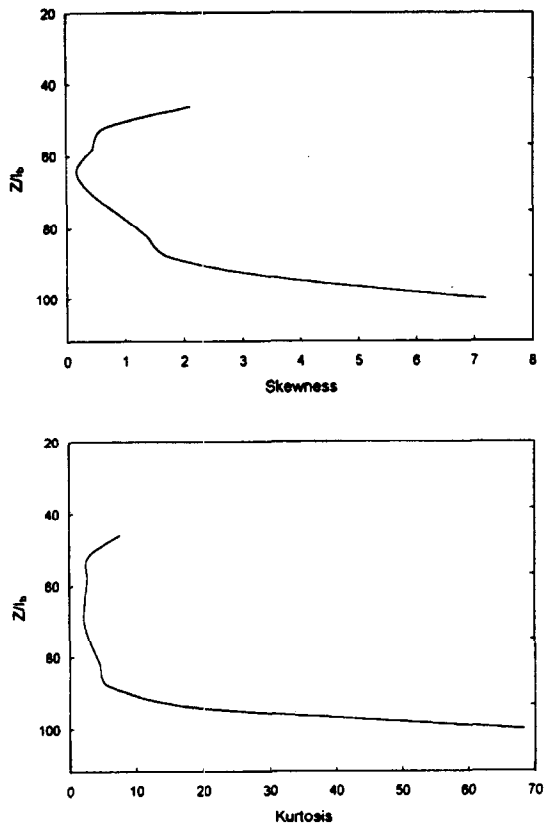

Fig. 8. Vertical profiles of skewness and kurtosis at $x/\ell_B = 240$, $y/\ell_B = 6$. $\ell_B = 0.077$ cm.

This is indeed the case. Values of skewness rise to approximately 10 in the region centered on $y/\ell_B = 24$, $z/\ell_B = 88$. Similarly, large values of kurtosis occur in the vicinity of the plume's perimeter. As may be expected, contours of higher moments are less smooth than those of the lower moments; also note that the logarithm ($\log_{10}$) of the kurtosis is plotted rather than the value of the kurtosis due to the large range of values.

Some insight on aspects of mixing processes can be inferred by constructing and analyzing a "conditional" signal. Figure 10 shows a schematic of how such a signal is formed. Following the approach of Wilson *et al.* (1985) the goal is to obtain a signal that contains only readings from when the plume is present at the probe. When the plume is absent the signal does not drop to zero due to noise. Thus a low threshold value is used to edit the signal so that any reading below the threshold is set to zero. These zero values are then removed from the signal, thus yielding the conditional signal. (In the results discussed below the value of the threshold was $\rho/\Delta\bar{\rho}_0 = 0.01$. Results using threshold values up to $\rho/\Delta\bar{\rho}_0 = 0.02$ were not markedly different.) Several quantities are then calculated and presented in Fig. 11 which shows crosswind distributions (i.e. y–z plane) at $x/\ell_B = 240$. These quantities are the total intensity $i = \rho'/\bar{\rho}$; conditional intensity $i_c = \rho_c'/\bar{\rho}_c$; intermittency factor

$$\gamma = 1 + i_c^2/1 + i^2 \tag{3}$$

burst frequency f_B determined by counting the number of bursts (i.e. large events above the threshold level) and dividing by the length of the time series; and burst persistence time γ/f_B. (In the above $\bar{\rho}_c$ and ρ_c' are the values of the mean and rms fluctuation of the conditional signal of the density time series.) In the presentation of the results the burst frequency and the burst persistence time have been non-dimensionalized by $\Delta Z/\bar{U}$, where ΔZ is the vertical extent of the plume and $\bar{U}$ is the crossflow velocity. (At $x/\ell_b = 240$ value of ΔZ is approximately 2.5 cm.)

Values of total intensity i are greater at the perimeter of the plume; for example, in Fig. 11a values increase from approximately 0.5 at the plume center to 1.75 at the perimeter. As the maxima of the density time series have similar values at the perimeter and center of the plume (recall Fig. 7), the distribution of total intensities of Fig. 11a arises from the greater number of events at the center of the plume: this raises the value of the means within the core so decreasing total intensities. Conditional intensities i_c of Fig. 11b are similarly distributed as total intensities albeit with a lower range of values from 0.3–0.6 as the mean value of a conditional signal is larger than the mean value of the corresponding total signal. Note that the magnitudes of the intensities i, i_c in Fig. 11a and b differ from the magnitudes of the intensities in Fig. 9. This arises from the normalization using $\Delta\bar{\rho}_0$ in Fig. 9a and b; in contrast, in Fig. 11a and b the normalization of the intensities at each location is by the value of the mean for the time series at that location (i.e. a local mean). The greater number of events at the plume center is reflected in higher values of intermittency γ. Figure 11c shows that the intermittency γ attains values about 0.85–1 at the plume's center (i.e. core), and 0.25–0.4 in the vicinity of the plume's perimeter. This implies that near the core there is almost always fluid from the plume present, while at the edges plume material is present for a fraction of the time only. Figure 11d shows that values of the non-dimensional burst frequencies also decrease towards the edge. Highest non-dimensional frequencies ≈ 1 occur in the vicinity of the core and the axis $y = 0$, and values decrease towards the edge. Events (or bursts) are thus more rare (or intermittent) at the edge. However, the average persistence time of the events are found to be approximately uniformly distributed (Fig. 11e). As the frequency distribution is inhomogeneous, the homogeneity of the burst persistence time suggests that both high frequency events of short duration, and low frequency events of long duration, contribute significantly to the production of fluctuations.

The variation of conditional intensity i_c with total intensity i is shown in Fig. 12. As may be expected,

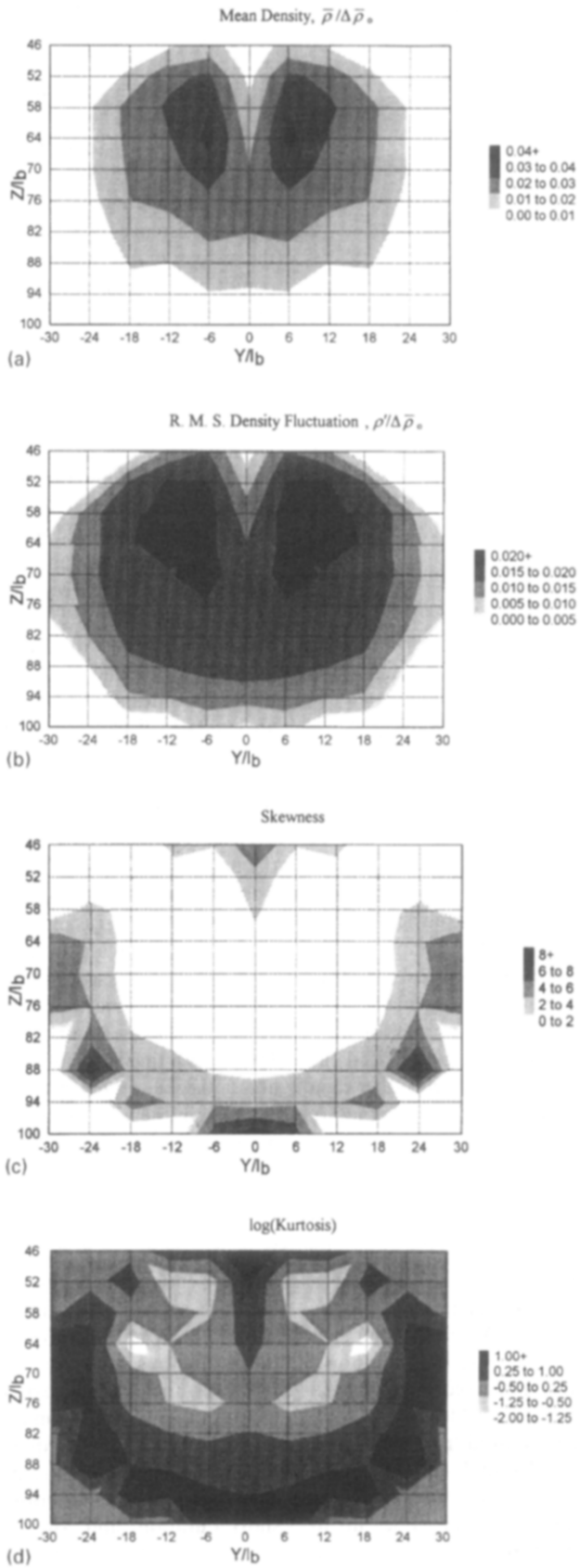

Fig. 9. Crosswind (i.e. y–z plane) profiles of mean density, rms density fluctuation, skewness and kurtosis at $x/\ell_B = 240$. $\ell_B = 0.077$ cm. Note that only data for values of $y \geqslant 0$ were obtained; data for negative values of y were generated by reflection.

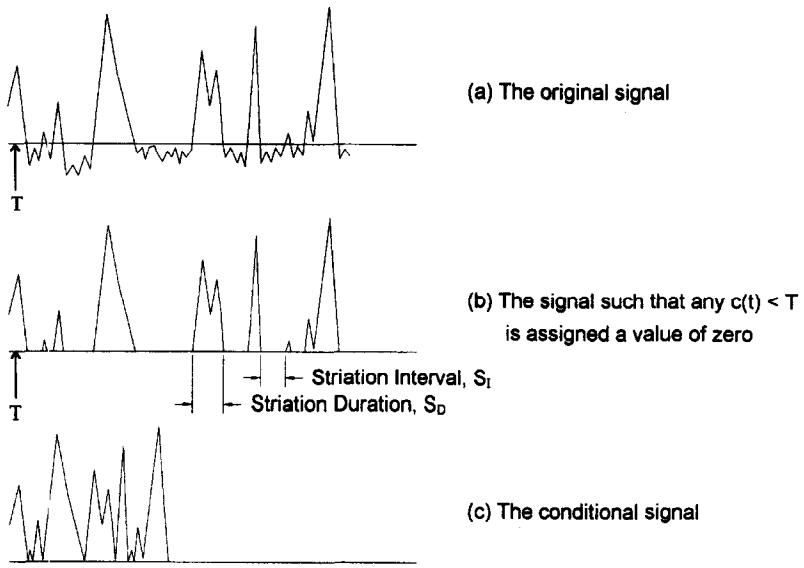

Fig. 10. Schematic for the formation of the conditional signal. Also shown are the definitions for striation duration and interval.

values of i_c are smaller than i, the data is scattered but show a weak increase in the value of i_c with increasing i. It is useful to compare values of fluctuation intensity for the present configuration of a buoyant bent-over plume with limiting cases such as a passive (i.e. in the absence of buoyancy forces) dispersing plume and a passive, round turbulent jet. For passive, round turbulent jets into a quiescent environment (i.e. no buoyancy, no meandering) Dowling and Dimotakis (1990) found values of $i \approx 0.23$ independent of distance on the jet centerline. For a crosswind line source (i.e. no meandering) Stretch (1986) found that magnitudes of fluctuations were similar for dense plumes and neutrally buoyant releases with maximum values of $i \approx 0.25$. Results for meandering plumes in the atmospheric boundary layer generally possess larger values of fluctuation intensity. For example, for large distances from the source Mylne and Mason (1991) found values of $i_c \sim 0.8$, $i \sim 1.1$; Jorgensen and Mikkelsen (1993) found $i_c \sim 1.5$, $i \sim 2.0$; Yee *et al.* (1993a) found $i_c \sim 1.0$, $i \sim 3.0$. Also shown is the empirical relationship for meandering plumes of Wilson and Zelt (1990) which is also discussed in Wilson (1995):

$$i_c = 2i/(2 + i)^2 . \tag{4}$$

Clearly the present data are bounded by equation (4). This is useful for it allows the calculation of the (upper bound) value of the intermittency γ via equation (3) and so facilitates an estimate of the fraction of the time that plume material exists at a location.

As for the total signal, it is possible to determine the skewness S_c and kurtosis K_c for the conditional signal. Figure 13 shows the present data for the conditional skewness and conditional kurtosis, and shows trends of increasing values of S_c and K_c with increasing values of conditional intensity i_c. Best-fit lines to the data for $i_c^2 > 0.3$ are well described by the simple expressions

$$S_c = 2.5\, i_c \tag{5a}$$

$$K_c = 9\, i_c . \tag{5b}$$

Trends differ for small values of $i_c^2 < 0.3$ and best-fit lines are described by

$$S_c = 200\, i_c^8 \tag{6a}$$

$$K_c = 60\, i_c^4 . \tag{6b}$$

Thus the data indicate that for small values of $i_c^2 < 0.3$ the nature of the statistics of the density fluctuations differs from those for large fluctuations $i_c^2 > 0.3$. The difference is attributable to the fact that data for $i_c^2 < 0.3$ occurs generally at the middle of the plume, whereas data for $i_c^2 > 0.3$ occurs mostly at the perimeter of the plume. A similar change for ground level fluctuations was also found by Yee *et al.* (1993b).

Stretching, folding and breaking of plume fluid elements by the strain field of the turbulence results in the creation of smaller scale plume fluid elements or striations. Insight on the scale of the striations can be obtained by considering the average duration of events (i.e. striation thickness S_D) and the average interval between the events, S_I, of time series of the density signals (see Fig. 10). For convenience, in the discussion below we present the data on striation duration and interval in units of time as the density field is advected past the probe. Vertical distributions of non-dimensional average striation duration and interval are plotted on Fig. 14 for three downstream

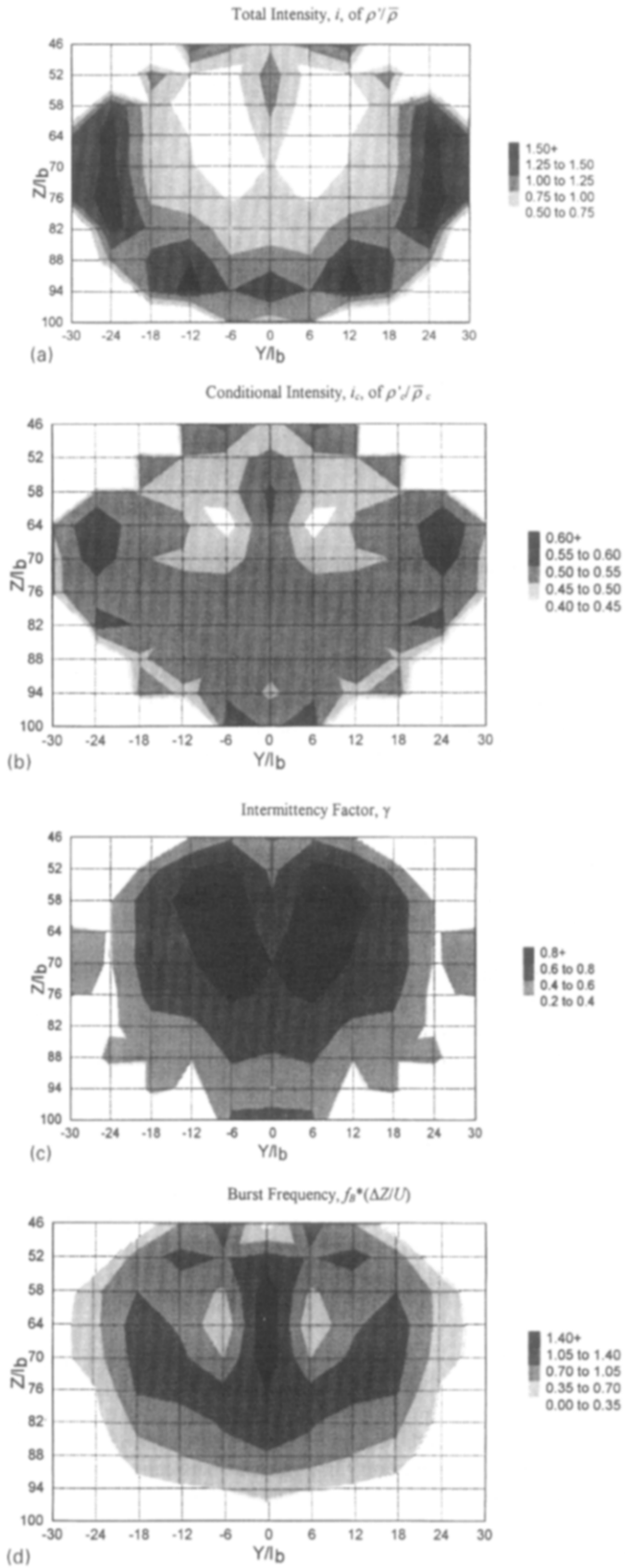

Fig. 11. Crosswind (i.e. y–z plane) profiles of the total intensity $\rho'/\bar{\rho}$, conditional intensity $\rho'_c/\bar{\rho}_c$, intermittency γ, non-dimensional burst frequency and burst persistence time at $x/\ell_B = 240$. $\ell_B = 0.077$ cm. Note that only data for values of $y \geqslant 0$ were obtained; data for negative values of y were generated by reflection.

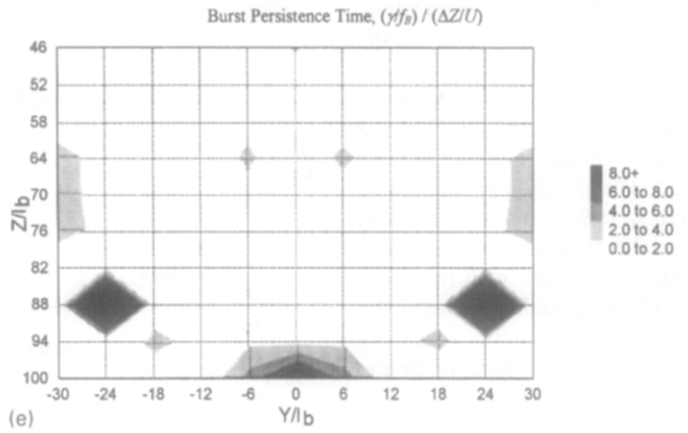

Fig. 11e.

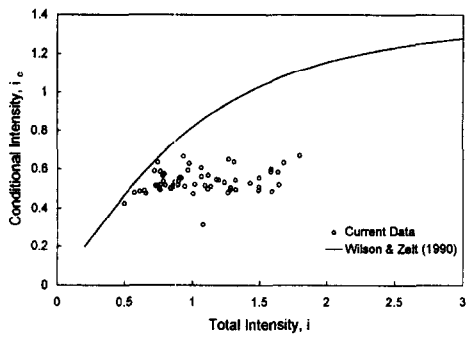

Fig. 12. Variation of the conditional intensity with total intensity. Data are a compilation from centerline to various off-axis locations. Also shown is the empirical correlation $i_c^2 = 2i^2/(2 + i^2)$ of Wilson and Zelt (1990).

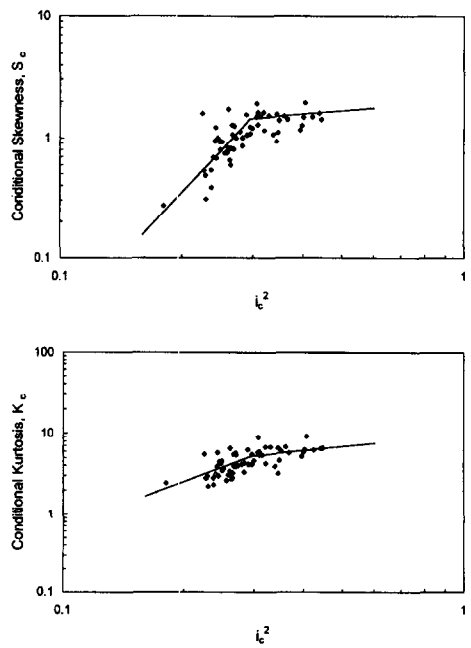

Fig. 13. Dependence of conditional skewness and conditional kurtosis with conditional intensity. Also indicated are lines described by equations (5) and (6). $\ell_B = 0.077$ cm.

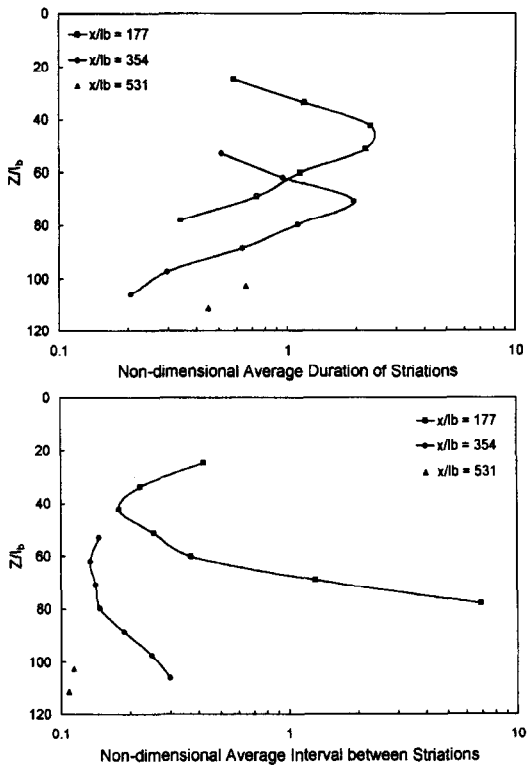

Fig. 14. Vertical profiles of average striation duration and interval at plume centerline (i.e. $y = 0$) at $x/\ell_B = 177$, 354, 531. $\ell_B = 0.056$ cm. Data are non-dimensionalized as $t/(\bar{U}/\Delta z)$.

locations. Figure 14a shows that values of the striation duration S_D reaches a maximum value at the same location as the mean densities (see Fig. 3, maxima for both $\bar{\rho}/\Delta\bar{\rho}_0$ and S_D occur at $z/\ell_b \approx 50$, 80 for $x/\ell_B = 177$, 354). That is, maximum values of striation duration occurs in the middle of the plume. (Dimensional values of the average striation duration decrease from a maximum value of about 0.4 s to less than 0.1 s at the plume's edges; for the data of Fig. 14b at the center of the plume the average striation interval, S_I, is approximately 0.05 s and is independent of

distance.) In contrast to average striation duration, Fig. 14b shows that average striation interval (i.e. the time or distance between events) increases towards the plume's edges. Note that at the plume center $S_I < S_D$ by an order of magnitude. Thus the time interval between puffs (i.e. parcels of plume fluid) is less than the duration of the puff. The situation is reversed at the plume's edges where $S_D < S_I$ so that the thickness or duration of puffs is smaller than the time interval or gap between puffs. This is consistent with the interpretation of Fig. 9a and b, that smaller values of the mean and fluctuation at the plume's edges arise from the decreased probability of occurrence of plume fluid.

Comparison of the magnitudes of S_D with the Kolmogorov timescale ($T_{KOL} = \nu/\varepsilon_p)^{1/2}$ provides further insight into mixing dynamics. Here ε_p is the mean dissipation rate of internally generated plume turbulence: data for ε_p are given in Fig. 9 of Huq and Stewart (1996). For present purposes, values of $T_{KOL} =$ 0.024, 0.053, 0.075 s at $x/\ell_B = 177$, 354 and 531 respectively for the data shown in Fig. 14. As values of S_D are 0.45, 0.56 and 0.28 s at the same locations, it is evident that the duration of the striations is greater than the scale of the smallest eddy of the turbulent field. When $S_D \gg T_{KOL}$ the smallest scale strain-rate fluctuations of the turbulent velocity field are relatively ineffective at deforming and breaking the scalar fluid elements of scale S_D into smaller elements because of the difference in scales of the scalar fluid elements and Kolmogorov scale eddies. Noting also that $S_D > S_I$, the schematic picture of the small scale scalar field for the data of Fig. 14 is of scalar fluid elements that are larger in size than the Kolmogorov scale eddies, with the average spacing between the scalar fluid elements being less than the size of the scalar fluid elements. For this schematic picture spectral densities of the scalar field are likely to be greater than the predictions of the inertial-convective subrange (Batchelor, 1959). Figure 15a shows that spectral densities are indeed greater, and that the decay is less steep (approximately -1) than the $-\frac{5}{3}$ slope of the inertial-convective sub-range. Note that over a similar range the companion spectrum of the velocity field (Fig. 15b) shows that the spectrum evolves with a $-5/3$ slope expected for an inertial sub-range.

Large scalar fluctuations may be expected to occur much less frequently for $S_D \approx T_{KOL}$ i.e. when the length scale of the scalar fluid elements is similar to the length scale of the smallest eddies of the turbulent velocity field. This is because when $S_D \approx T_{KOL}$ the smallest scale turbulent eddies are efficient at stretching and breaking similarly sized scalar fluid elements thereby enhancing rates of molecular mixing. An estimate of the ratio of the scale of the fluid elements to the scale of the Kolmogorov scale eddy is given by the value of the ratio S_D/T_{KOL}. This ratio is plotted on Fig. 16. The data show that from initially large values the ratio S_D/T_{KOL} decreases with increasing values of x/ℓ_B. The greater the value of the ratio S_D/T_{KOL} the

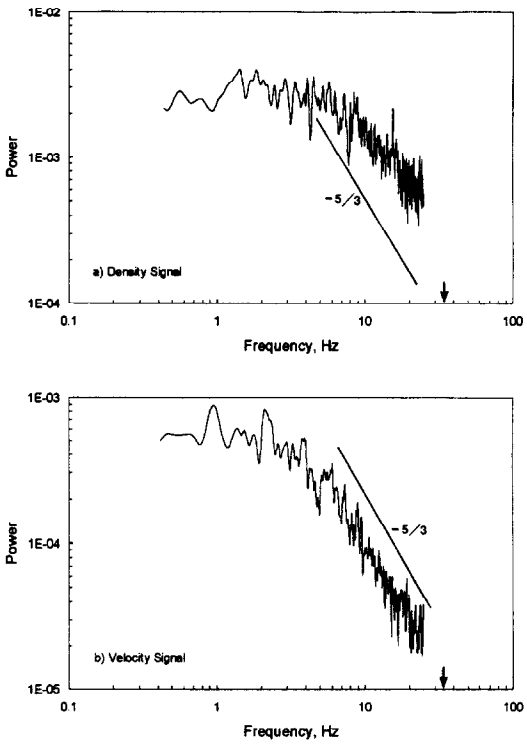

Fig. 15. Frequency spectra for density and velocity signals at ($x/\ell_B = 240$, $y/\ell_B = 0$, $z/\ell_B = 70$). Indicated is $-\frac{5}{3}$ power law slope, and an arrow for the Kolmogorov timescale. Nyquist frequency is 25 Hz. $\ell_B = 0.077$ cm.

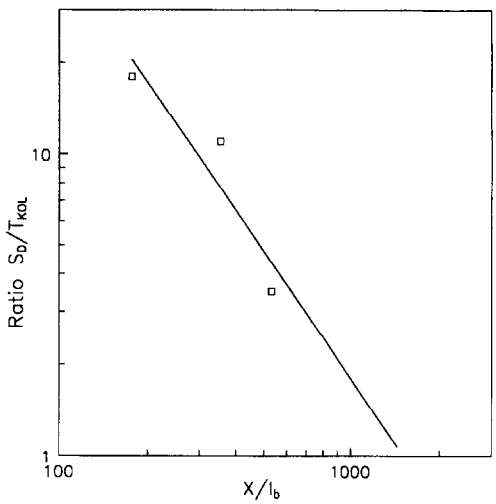

Fig. 16. Evolution of S_D/T_{KOL}, the ratio of striation duration to Kolmogorov timescale, with downwind distance x/ℓ_B.

greater is the range of frequencies, or eddy sizes which contribute towards distorting or breaking scalar (or density) fluid elements. Thus the turbulent field is relatively most efficient at mechanical breakage of large scale scalar fluid elements when S_D/T_{KOL} is largest.

With increasing distance the ratio S_D/T_{KOL} decreases to $S_D/T_{KOL} \approx 1$ at $x/\ell_B \approx 1500$. In comparison to conditions for $S_D/T_{KOL} \gg 1$, for $S_D \approx T_{KOL}$ the primary action of the largest scale eddies is to advect the much smaller scale scalar fluid elements. Thus only the small (Kolmogorov) scale strain-rate fluctuations are relatively effective at deformation and breakage; the result is reduced efficiency, as regards deformation and breakage, and the creation of sufficiently large scalar gradients to facilitate molecular diffusion. For these high Schmidt number experiments the smallest scalar fluid elements can be smaller than Kolmogorov sized eddies: for such small scales the predominant action of Kolmogorov scale eddies is advection rather than breakage. Thus, schematically, the evolution of the scalar field for high Schmidt number flows can be delineated as efficient mechanical breakage down to Kolmogorov scales and diffusion for scales between the Kolmogorov scales and the Batchelor scale $(\varepsilon/\nu D^2)^{1/4}$. Obviously breakage will occur of scalar fluid elements between the Kolmogorov and Batchelor scales, but it will be at a slower rate than for scalar fluid elements larger than the Kolmogorov scale. For typical problems of discharge of gases to the atmosphere the value of the ratio of momentum to thermal diffusion (Prandtl number) is approximately 1, and Fig. 16 is a useful upper bound estimate for distances when concentration fluctuations are likely to be significant. Our measurements and analysis suggest that significant levels of scalar fluctuations, albeit of short duration, are likely to be a characteristic of the scalar field even for distances where magnitudes of mean concentration are as small as 1% of the original value at the source (recall Figs 3 and 6). Thus evaluation of toxicity or flammability arising from steady, buoyant plumes in a crossflow should consider the likelihood of large, instantaneous scalar fluctuations for distances at least up to $x/\ell_B \approx 10^3$.

5. CONCLUSIONS

Although the flow field of a steady, buoyant plume in crossflow is common, there is little previous data on the turbulent density field. In particular, little is known about the nature and magnitude of density fluctuations despite their likely role in influencing hazard assessments of toxicity or flammability. This experimental study has been undertaken to address this shortcoming. Data from long time series of the fluctuating density field and high density traverses are used to discern the nature and distribution of the statistics of turbulent density fluctuations throughout the plume.

Mean density measurements show that the crosswind structure (i.e. in the y–z plane) of the buoyant plume comprises two high density cores: the maximum mean density $\Delta\bar{\rho}_{MAX}$ at a downwind location occurs approximately in the center of these high density cores. Values of $\Delta\bar{\rho}_{MAX}$ diminish rapidly with distance x/ℓ_B from the source due to entrainment (e.g. values of $\Delta\bar{\rho}_{MAX}$ are about 2% of $\Delta\bar{\rho}_0$, the value at the source, by $x/\ell_B \sim 500$). Root mean square levels of density fluctuations attenuate quickly as $\rho'/\Delta\bar{\rho}_0 = 8(x/\ell_B)^{-1}$. However, values of ρ' are similar in magnitude to the local mean value of $\Delta\bar{\rho}_0$ so that at the center of the plume $\rho'/\Delta\bar{\rho}_{MAX} \approx 0.85$ for all downwind locations.

Time series of the density signals were intermittent at both the center of the high density core and at the edge of the plume. It is found that the magnitudes of the peak or extreme values of the density time series are similar at the center of the high density core and plume edge and is an order of magnitude greater than the mean. This indicates that mean concentrations and fluctuations are determined by the probability of locating plume material at a given point; that is, distributions are determined by the frequency of events rather than variations in the intensities of events. Spatial distributions of the values of skewness and kurtosis show approximately Gaussian values in the middle of the high density core: larger values of skewness (~ 10) and kurtosis ($K \sim 100$) indicate skewed and peaked distributions at the edge of the plume.

Analysis of the conditional signal of the density time series showed that the magnitude of the conditional intensity i_c is in accord with the empirical relationship $i_c^2 = 2i^2/(2 + i^2)$. Peak values of the conditional intensity were about 0.6. Spatial distributions show that values of the intermittency γ and the non-dimensional burst frequency $f_B(\Delta Z/\bar{U})$ decreased towards the edge of the plume: in contrast, values of the non-dimensional burst persistence time $(\gamma/f_B)/(\Delta Z/\bar{U})$. were approximately uniform through the plume.

Evaluation of the duration of the events and the time between events of the density time series revealed that the average striation duration S_D is greater than the average striation interval S_I between events at the middle of the core. Thus the structure of the turbulent density field at the core center is one of relatively densely packed plume fluid elements with the consequence of elevated spectral densities. The average striation duration decreases with downwind distance, and approach Kolmogorov microscales at distances of order $x/\ell_B \sim 10^3$. This suggests that instantaneously large density fluctuations will persist for distances at least up to $x/\ell_B \sim 10^3$.

Acknowledgements—Financial support from E. I. DuPont de Nemours, Inc. and Sterling Diagnostics Inc. is gratefully acknowledged.

REFERENCES

Bara, B. M., Wilson, D. J. and Zelt, B. W. (1992) Concentration fluctuation profiles from a water channel simulation of a ground-level release. *Atmospheric Environment* **26A**, 1053–1062.

Batchelor, G. K. (1959) Small-scale variation of convected quantities like temperature in turbulent fluid. Part I. General discussion and the case of small conductivity. *J. Fluid Mech.* **5,** 113–133.

Deardorff, J. W. and Willis, G. E. (1984) Groundlevel concentration fluctuations from a buoyant and a non-buoyant source within a laboratory convectively mixed layer. *Atmospheric Environment* **18,** 1297–1309.

Devaull, G. E. (1990) Fluctuating concentrations in atmospheric dispersion. Ph.D. thesis, Department of Mechanical Engineering, University of Illinois at Urbana-Champaign, Urbana, Illinois.

Dinar, N., Kaplan, H. and Kleiman, M. (1988) Characterization of concentration fluctuations of a surface plume in a neutral boundary layer. *Boundary-Layer Met.* **45,** 157–175.

Dowling, D. R. and Dimotakis, P. E. (1990) Similarity of the concentration field of gas phase turbulent jets. *J. Fluid Mech.* **218,** 109–141.

Fackrell, J. E. and Robins, A. G. (1982) Concentration fluctuations and fluxes in plumes from point sources in a turbulent boundary layer. *J. Fluid Mech.* **117,** 1–26.

Hanna, S. R. (1984) The exponential probability density function and concentration fluctuations in smoke plumes. *Boundary-Layer Met.* **29,** 361–375.

Huq, P. and Stewart, E. J. (1996) A laboratory study of buoyant plumes in laminar and turbulent crossflows. *Atmospheric Environment* **30,** 1125–1135.

Jones, C. D. (1983) On the structure of instantaneous plumes in the atmosphere. *J. Haz. Mat.* **7,** 87–112.

Jorgensen, H. E. and Mikkelsen, T. (1993) Lidar measurements of plume statistics. *Boundary-Layer Met.* **65,** 361–378.

Lewellen, W. S. and Sykes, R. I. (1986) Analysis of concentration fluctuations from lidar observations of atmospheric plumes. *J. Clim. appl. Met.* **25,** 1145–1154.

List, E. J. (1982) Turbulent buoyant jets and plumes. In *Mechanics of Turbulent Buoyant Jets and Plumes* (edited by Rodi W.), pp. 1–68. Pergamon Press, Oxford.

Mylne, K. R. (1993) The vertical profile of concentration fluctuations in near-surface plumes. *Boundary-Layer Met.* **65,** 111–36.

Mylne, K. R. and Mason, P. J. (1991) Concentration fluctuation measurements in a dispersing plume at a range of up to 1000 m. *Q. Jl. R. Met. Soc.* **117,** 117–206.

Sawford, B. L. (1987) Conditional concentration statistics for surface plumes in the atmospheric boundary layer. *Boundary-Layer Met.* **38,** 209–223.

Sawford, B. L., Frost, C. C. and Allan, T. C. (1985). Atmospheric boundary-layer measurements of concentration statistics from isolated and multiple sources. *Boundary-Layer Met.* **31,** 249–268.

Stretch, D. D. (1986) The dispersion of slightly dense contaminants in a turbulent boundary layer. Ph.D. Thesis, Department of Engineering, University of Cambridge.

Wilson, D. J. (1995) Concentration fluctuations and averaging time in vapor clouds. Center for Chemical Process Safety, American Institute of Chemical Engineers, New York.

Wilson, D. J. and Simms, B. W. (1985) Exposure time effects on concentration fluctuations in plumes. Report No. 47, Department of Mechanical Engineering, University of Alberta, Edmonton, Canada.

Wilson, D. J. and Zelt, B. W. (1990) Technical basis for EXPOSURE-1 and SHELTER-1 models for predicting outdoor and indoor exposure hazards from toxic gas releases. Report No. 72, Department of Mechanical Engineering, University of Alberta, Edmonton, Canada.

Wilson, D. J., Robins, A. G. and Fackrell, J. E. (1985) Intermittency and conditionally averaged concentration fluctuation statistics in plume, *Atmospheric Environment* **19,** 1053–1064.

Yee, E., Kosteniuk, P. R., Chandler, G. M., Biltoft, C. A. and Bowers, J. F. (1993a) Statistical characteristics of concentration fluctuations in dispersing plumes in the atmospheric surface layer. *Boundary-Layer Met.* **65,** 69–109.

Yee, E., Wilson, D. J. and Zelt, B. W. (1993b) Probability distributions of concentration fluctuations of a weakly diffusive passive plume in a turbulent boundary layer. *Boundary-Layer Met.* **64,** 321–354.